LRP 668/00   June 2000

Divertor Geometry Effects
on Detachment in TCV

R.A. Pitts, B.P. Duval, A. Loarte, J.-M. Moret,
J.A. Boedo, D. Coster, I. Furno, J. Horacek,
A.S. Kukushkin, D. Reiter, J. Rommers
and the TCV Team

Divertor Geometry Effects on Detachment in TCV

R.A. Pitts, B.P. Duval, A. Loarte[a], J.-M. Moret, J. A. Boedo[b], D. Coster[c], I. Furno, J. Horacek[d], A. S. Kukushkin[e], D. Reiter[f], J. Rommers and the TCV Team[*]

Centre de Recherches en Physique des Plasmas,
Association EURATOM-Confédération Suisse,
École Polytechnique Fédérale de Lausanne, CH-1015 Switzerland

[a]*EFDA-CSU, Max Planck Institut für Plasmaphysik, D-85748 Garching, Germany*
[b]*Fusion Energy Program, University of California, San Diego, CA 92093-0417, USA*
[c]*Max-Plank-Insitut für Plasmaphysik, Boltzmannstr. 2, D-85748, Garching, Germany.*
[d]*IPP, Academy of Sciences of the Czech Republic, Za Slovankou 3, POB 17, 182 21 Praha*
[e]*ITER Joint Central Team, Garching Joint Working Site, Boltzmannstr. 2, D-85748, Garching, Germany.*
[f]*Institut für Laser und Plasmaphysik, Heinrich-Heine-Universität Düsseldorf, Universitätsstr.1, D-40225 Düsseldorf, Germany*

Abstract

Experimental observations and some preliminary results from code modelling of divertor detachment in the TCV tokamak are reported, with emphasis on the aspects of this detachment related to divertor geometry. The contribution is restricted to deuterium fuelled, ohmic plasmas for which the ∇B drift is directed away from the X-point of lower single-null, open diverted equilibria with fixed elongation and triangularity. Unlike more conventional diverted equilibria, however, the configurations described are characterised by both a very short divertor poloidal depth on a vertical target and a very long poloidal depth on a horizontal target. Results are presented from density ramp discharges in which the outer (high poloidal depth) divertor is already in the high recycling regime at the start of the density ramp and in which varying degrees of detachment are obtained depending on the magnitude of the imposed outer divertor flux expansion. In contrast, the inner divertor remains in the large part attached for all densities. Many of these features are reproduced by simulations using the B2-Eirene code package, leading to some interesting insights into how the relatively low divertor densities observed and predicted for TCV (compared with larger machines) can nevertheless yield a recombination ion sink sufficient to explain the observed outer target detachment. The code results demonstrate, in addition, how misleading divertor target Langmuir probe measurements of T_e during detachment in TCV can be.

---

*. For the full list of authors see, for example, ref. [1]

1. Introduction

The existing coil set and first wall design impose short X-point to central column distances for diverted discharges created in the TCV tokamak ($R = 0.89$ m, $a = 0.25$ m, $B_\varphi = 1.43$ T). In turn, this requires that at least one of the divertor legs in single-null equilibria be poloidally rather short, although considerable freedom exists for modifying the magnetic geometry of the low field side (LFS) divertor leg. One particular configuration is used as a base for divertor physics studies in TCV (see Fig. 1) and was presented in an earlier paper in connection with detachment studies using neon seeding [2]. The latter was required since detachment using deuterium fuelling alone could not otherwise be achieved. Following the TCV first wall upgrade in late 1998 [3], the detached state was obtained in D_2 alone, leading to speculation that this may be linked to the increased surface coverage of carbon protection tiles (from $\approx 65\%$ to $\approx 90\%$ of internal surface area) afforded by the in-vessel modifications. This contribution presents some of the first experimental observations of this detachment, with particular emphasis on the role of divertor geometry, together with the results of some preliminary simulations of the experiments using the B2-Eirene code package.

2. Experiment

Figure 1 illustrates the three equilibria discussed in this contribution. All have $\kappa_{95} = 1.6$, $\delta_{95} = 0.35$ and fixed X-point height, $z_{Xpt} = 57$ cm, defined as the vertical distance from the X-point to the vessel floor. The emphasis here is on the effect of outer divertor flux expansion, f_{exp}, the values of which close to the separatrix are noted on the figure for the specific discharges and which fall in the general range $f_{exp} = 2.5 \rightarrow 10$ for all shots of this type executed thus far. This should be compared with the value at the inner target, fixed at 4.0 for all equilibria. Experiments have been performed in ohmic plasmas only with unfavourable $B \times \nabla B$ drift direction and plasma current, $I_p = 340$ kA, corresponding to $q_{95} = 2.9$. Under these conditions, the midplane to outer target parallel connection length near the separatrix is ≈ 25 m with $\approx 70\%$ of this appearing in the poloidal distance, z_{Xpt}. In contrast, whilst the outer midplane to inner target connection lengths are comparable to the LFS divertor target, the inner X-point to target poloidal distance is only some 8 cm, corresponding to only ≈ 2.5 m parallel to the total field. An interesting feature of these configurations is the unavoidable presence in the same discharge of

both a horizontal and a vertical target zone.

Much of the data discussed here originate from two arrays of single Langmuir probes and a fast reciprocating probe, the positions of which are also indicated in Fig. 1. The divertor target arrays comprise 26 and 34 spherical tip, cylindrical graphite single probes of diameter 4.0 mm, embedded in the outer and inner target tiles and with spatial resolutions of 11.0 mm and 17.0 mm respectively. The fast probe [4] enters the plasma edge at the tokamak midplane and makes two reciprocations per discharge, with the peak of the first movement at the beginning of the density ramp at 0.6 s and the second at 1.0 s when detachment has begun at the outer target. The current probe configuration is an array of five separate graphite pins, with both tip length and diameter = 1.5 mm. Two were operated as swept single probes for these experiments. At present the diagnostic has no Mach probe capability, but this is planned.

Figure 2 summarises the typical density ramp discharge showing many of the characteristics seen during divertor detachment under similar conditions in other devices [5-8]. All of the examples described here terminate in disruption when $\bar{n}_e \approx 65\%$ of the Greenwald limit and the ratio $P_R^{OUT}/P_\Omega \approx 0.8$ (Fig. 2(c)). This does not, however, appear to be specifically linked to any particular movement of the radiation distribution around the X-point which, from relatively early on in the density ramp is localised at the X-point. In fact, in most cases, the disruption occurs a few 10's of ms after the current plateau when the outer divertor leg is beginning to move back up the central column (although the density is still rising). The divertor radiation, P_R^{DIV}, saturates quickly after the density ramp begins, corresponding to the establishment of a high recycling regime at the outer target (note in Fig. 2(f) the plateau on the ion saturation current density of a probe located close to the outer strike point). This is simply due to the low temperatures established throughout the divertor volume, such that most of the radiation originates from the X-point region where T_e is sufficiently high for carbon (the dominant impurity in TCV) to radiate strongly. At around 0.75 s, when, for this particular dicharge, $\bar{n}_e = 7.5 \times 10^{19} m^{-3}$, the separatrix target ion flux begins to fall, and shortly afterward the D_α emission in the region near the outer target (Fig.2(e)) begins to increase rapidly. One may also note the extremely low Z_{eff} of these plasmas, and in particular, the steady decrease in Z_{eff} as $\bar{n}_e$ increases and detachment proceeds.

3. Divertor and SOL Measurements

3.1 Target Probes

Whilst not showing the details of the profile shape across the target, the time space plots of target parallel ion current density, j_{sat}, in Fig. 3 are useful in showing qualitatively how the character of detachment differs with increasing flux expansion at the outer target. At low f_{exp}, detachment begins first near the separatrix, occurring further out in the SOL at progressively higher $\bar{n}_e$. For regions deep into the divertor fan, the ion flux continues to increase but the absolute values are small compared with those at the separatrix. In addition, the probes there lie on flux surfaces which intersect the outer wall before arriving at the outer midplane. As f_{exp} increases, detachment begins only marginally earlier in density at the separatrix, but then extends much deeper into the divertor fan and occurs at a more leisurely pace. At the highest densities, the current to all probes has decreased and detachment is complete across the outer target.

The increase in f_{exp} implies a decrease in total magnetic field line angle at the target, the average of which across the the target decreases in the ratio 3.5°:1.25°:0.75° for the values of f_{exp} = 2.8:6.4:9.3 in Fig. 1. For very small angles, significant probe shadowing occurs by neighbouring tile edges, the alignment of which on the TCV vessel floor is not guaranteed to better than 0.5 mm. These shadowing effects are the cause of the apparent "hole" in the profile at ≈ 10 cm from the separatrix at the highest f_{exp}.

At the inner target, except at the very highest $\bar{n}_e$ and close to the separatrix, the plasma remains attached throughout, with separatrix particle flux densities a factor 3-3.5 higher than those at the outer target, independent of flux expansion. This feature is reproduced by the code simulations, without accounting for drifts in the SOL, and is most likely linked to the vertical plate geometry.

A more quantitative basis for comparison of these target ion fluxes is obtained by using them to compute a Degree of Detachment, DOD [5], describing the extent to which the ion flux obeys the scaling, $\Gamma \propto \bar{n}_e^2$ predicted by the basic Two-Point Model [9] of the divertor for the high recycling regime (the use of $\bar{n}_e$ assumes proportionality between the core and upstream separatrix densities). By normalising to the values at the beginning of each density ramp, DOD's have been computed at both targets for the separatrix ion current density and the integrated ion current normal to the tiles across the strike zones. The results are collected in Fig.

4 for the series of three outer flux expansions in Fig. 1. When the DOD $\gg$ 1, detachment is occurring and one may note from Fig. 4 the trends already discussed above. At lower f_{exp}, separatrix detachment occurs rapidly and is quickly complete, whilst with increasing f_{exp}, the separatix DOD reaches lower values and does so more slowly. In the meantime, the integral DOD's increase with f_{exp} indicating the greater extent of detachment at higher flux expansion. At higher I_p, the same trends are observed, but with lower absolute values of the DOD's and with detachment beginning at higher densities.

3.2 Reciprocating Probe

Figure 5 combines target and reciprocating probe profiles of electron density, temperature and pressure mapped to the outer midplane for the equilibrium with lowest outer flux expansion. The profiles are plotted in terms of distance from the magnetically located separatrix position, with the target profiles the result of averaging over 30 ms, centred on the time of maximum insertion point during the fast probe reciprocation. The earlier time correponds to high recycling with $\bar{n}_e = 7 \times 10^{19}$ m^{-3} and the second movement at 1.0 s to $\bar{n}_e = 1 \times 10^{20}$ m^{-3} when detachment is well advanced (see Fig. 3). Reassuringly, whilst the outer target profiles in particular change considerably with flux expansion, the upstream measurement remains largely unaffected by increasing f_{exp}.

An immediately obvious feature is the SOL density broadening during detachment and the apparent shift of the peak in the inner target T_e profile at high density, again probably related to the vertical target geometry and proximity of the X-point. One may also note the abrupt change in gradient of all signals at the location of the dashed vertical lines. The latter indicate the outer wall tile radius at the midplane so that data points at radii exceeding this location correspond to plasma on field lines intersecting the outer wall before arriving at the midplane. Since the fast probe has currently no Mach probe capability nothing can be said at this time regarding plasma flow in the SOL.

Within experimental errors, pressure balance appears to be reasonably satisfied during high recycling and detachment at the inner target but not at higher density for the outer target, as might be expected. It is significant, however, that outer target densities during detachment are considerably lower than upstream values, whilst downstream and upstream temperatures are similar. Since $n_e \propto 1/\sqrt{T_e}$, this leads one naturally to speculate on the validity of the T_e obtained from these divertor probes under such conditions, particularly in view of the code

results presented in Section 4 showing that the local T_e is considerably lower than measured (< 2 eV at the outer target compared with measurements in the range 5-20 eV). Such speculation is nothing new [10,11] and there are strong arguments for the case of the TCV divertor in support of significant deviations of the measured T_e from the real value local to the outer target under detached conditions [12]. These arguments are strengthened by observations (not shown here) at very low $\bar{n}_e$ (and hence high T_e) in which pressure balance is closely satisfied throughout the SOL.

3.3 Visible Emission Reconstructions

In recent years two-dimensional measurements of visible line radiation using CCD camera technology have become increasingly popular [13]. After suitable inversion [14], the resulting distributions offer interesting insight into the dynamics and localisation of the radiation and are useful for comparison with 2D code simulations. The system on TCV [14] tangentially views the lower half of the vacuum vessel encompassing both divertor strike zones for the configurations shown in Fig. 1 and permits observations (not yet simultaneously) of D_α emission at 656 nm and CIII emission at 465 nm. Recent 2D observations of CIV line radiation (155 nm) in DIII-D, from which most of the radiation power from carbon is expected to come, have shown that the CIV distribution is qualitatively similar to that of CIII [15].

The behaviour of CIII emission during the density ramp experiments described here is consistent with simple expectations based on cooling of the divertor volume with increasing $\bar{n}_e$. It is independent of outer divertor flux expansion and two examples, at the beginning and end of the density ramp for a discharge with $f_{exp} = 2.5$ are shown in Figs. 6(a,b). At low $\bar{n}_e$, the emission extends almost to the outer target and is most intense at the inner strike zone where T_e and presumably carbon sputtering is higher. At the highest density, the emission is concentrated on or just inside the outer separatrix and to a lesser extent near the X-point. This separatrix distribution is qualitatively expected based on the magnitude of T_e measured by the fast reciprocating probe (Fig. 5) in this region.

In the case of the D_α emission, Figs. 6(c,d,f) illustrate the spatial distributions observed as f_{exp} increases (the same sequence of equilibria as in Fig. 1). To isolate any geometry effects, such comparison must be made on the basis of a similar degree of detachment. This has been performed by using the experimental outer target integral DOD curves of Fig. 4 and extracting the DOD found at highest density for the lowest flux expansion (the value is $\approx$ 60). The

reconstructions plotted at higher flux expansion are thus extracted from CCD camera measurements made at the densities corresponding to this value. Such normalisation clearly shows that for lower f_{exp}, the emission extends to considerable vertical distances above the target but remains localised at the target for higher flux expansion. One may also note the apparent shift of the peak target intensity away from the separatrix as f_{exp} increases. Within the errors of CCD camera misalignment and the uncertainty in flux surface positions from the equilibrium reconstruction, the peak in the D_α profile along the target approximately coincides with that of the parallel ion flux density measured by the target probes at all values of f_{exp}. The reconstructions clearly demonstrate the effect of "plasma plugging" by the expanded flux surfaces as f_{exp} increases.

4. Comparison with B2-Eirene Code Simulations

Preliminary attempts at simulating the data presented in Section 3 have concentrated on just two values of outer target flux expansion with f_{exp} = 2.8 and 6.4. The simulations have been performed using the B2-Eirene code [16] on TCV discharge numbers #15445 and #15448, identical in all respects to #17824 and #17823 of Fig. 1 respectively, with the only difference being the availability of inner target and reciprocating probe data for the later shots. As a first approximation in order to see trends, the power crossing the separatrix has been fixed at 0.48 MW for all densities and for both equilibria. Likewise, a chemical sputtering yield, Y_{chem}= 1.5%, has been chosen, arbitrarily, with $D_\perp$ = 0.35 m^2s^{-1} and $\chi_\perp$ = 0.85 m^2s^{-1} providing reasonable agreement with target profile shapes. Such parameters tend to overestimate the measured target ion fluxes (even for the case of low f_{exp} when field line impact angles are high and the target probes more likely to be reliable - Section 3.1). One reason for this may be the choice of a too low Y_{chem}, since a higher value would lead to more radiation for a given density, less energy available for ionisation and hence lower target currents. No inward pinch has been applied in the code and no drifts are included.

The initial code runs have highlighted the importance, in the case of TCV, of elastic friction between D_2 molecules and D^+ ions [17] which serves to slow ions down sufficiently in the region between the ionisation front and the target such that significant recombination can occur. Without this additional momentum loss (along with that due to to ion-neutral charge-exchange), the relatively low densities in the TCV divertor would not produce enough recombination to

explain the observed detachment. With this effect switched on, the code yields $\approx 80\%$ recombination of the target ion flux at the highest densities (before a MARFE appears in the simulation) for high f_{exp}, but is not yet able to account for the level of detachment seen experimentally at low f_{exp}.

A selection of code results is summarized in Fig. 7, with the emphasis on direct comparison with the experimental data presented in Section 3. The computed distributions of D_α line emission appear in Fig. 7(a,b) for low and high f_{exp} respectively, showing very reasonable agreement with the measured spatial distributions of Fig.6 (c,d). In similar fashion to the experimental data, the code distributions are presented for the same absolute levels of total recombination. There is particularly striking agreement between theory and experiment with regard to the differences in vertical extent of the emission in passing from low to high f_{exp}. The indications are that this is likely due to more uniform distribution of momentum losses further up the outer leg owing to the greater neutral transparency of a laterally "thinner" divertor. Good agreement is also obtained between the code and experiment with regard to the movement of the CIII light emission as detachment progresses, independent of flux expansion. Similarly, the absolute value and dependence on density of Z_{eff} (Fig. 2(b)) are well matched by the simulations.

Code and experiment differ, however, with respect to the localisation of D_α emission at the target. Whilst the simulation places the highest intensity at the strike point and even into the private region, experiment shows the emission to be localized further out in the divertor fan, especially at high f_{exp}. This behaviour is not currently understood, but one might speculate as to the relative importance of molecular effects in the process of detachment. Whilst preliminary stand-alone Eirene simulations including a more refined treatment of deuterium molecules seem to indicate that their role might actually to be in reducing the predicted level of recombination (see also [18]), new calculations [19] point to a potentially important source of increased volume recombination involving proton charge exchange with hydro-carbon molecules. The latter might be expected to be present in large numbers in the TCV divertor plasma.

Figure 7(c) presents code results for the integral and separatrix DOD at low and high f_{exp} for direct comparison with Fig.4(a,b). Agreement in absolute value is excellent, but, interestingly, the code is unable to reproduce the very high separatrix DOD seen experimentally at low f_{exp}. Theory does, however, correctly simulate the generally higher DOD's at high f_{exp}.

Finally, Fig. 7(d) compares the simulated SOL and target electron pressure profiles for low

f_{exp} and under detached conditions. At present, the simulation grid in the SOL extends only to those magnetic surfaces not intersecting the vacuum vessel walls at the plasma midplane. The experimental upstream data are replotted from Fig. 5 at t = 1.0 s, whilst the measured target pressure has been recomputed using the measured parallel ion flux, but replacing the experimental T_e with the fixed value of 1 eV across the target predicted by B2-Eirene at this density. Athough theory and experiment do not coincide in absolute value (for reasons alluded to above), the *ratios* between upstream and target pressures in both cases are in very close agreement. This would seem to be a very convincing demonstration of the caution one should exercise in deriving T_e from target Langmuir probes under high recycling conditions, at least in TCV.

5. Conclusions

This contribution has addressed the nature of plasma detachment in extremely open diverted configurations in the TCV tokamak, with emphasis on the effect of magnetic flux surface expansion at the outer target of deuterium fuelled ohmic discharges with unfavourable BxVB drift direction. Upstream and target Langmuir probe data, together with tomographically inverted visible CCD camera measurements of deuterium and carbon line emission are in good qualitative, and often quantitative, agreement with preliminary B2-Eirene code simulations demonstrating enhanced degrees of detachment as flux expansion is increased and clearly showing the effects of plasma plugging by expanded flux surfaces. Whilst the outer divertor, with high poloidal depth and a horizontal target, detaches readily, the inner divertor plasma, with X-point to target distances a factor of 7 shorter remains attached, except very close to the strike point, even at the highest densities. Comparison of code and experiment shows convincingly that target Langmuir probe measurements of local electron temperature can be in error by large factors under conditions of high recycling and detachment.

Acknowledgements

References

[1]   O. Sauter et al., Phys. Rev. Lett., **84** (2000) 3322

[2]   R. A. Pitts et al., J. Nucl. Mater., **266-269** (1999) 648

[3]   R. A. Pitts, R. Chavan and J.-M. Moret, Nucl. Fusion **39** (1999) 1433

[4]   J. A. Boedo et al., Rev. Sci. Instr. **69** (1998) 2663

[5]   A. Loarte et al., Nucl. Fusion **38** (1998) 331

[6]   B. Lipshultz et al., J. Nucl. Mater **220-222** (1995) 50

[7]   T. W. Petrie, et al., Nucl. Fusion **37** (1997) 321

[8]   N. Asakura et al., J. Nucl. Mater. **241-243** (1997) 559

[9]   M. Keilhacker et al., Phys. Scr. **T2/2** (1982) 443

[10]   P. C. Stangeby, Plasma Phys. Contr. Fusion, **37** (1995) 1459

[11]   J. Wesson, ibid. 1031

[12]   J. Horacek, R. A. Pitts and A. Loarte, in preparation

[13]   M. E. Fenstermacher et al., Phys. Plasmas **4** (1997) 1761

[14]   B. P. Duval et al., Bull. Amer. Phys. Soc., **44** (1999) GP1 75

[15]   M. E. Fenstermacher et al., 26th EPS Conf. on Contr. Fusion and Plasma Phys., Maastricht, 14-18 June 1999, ECA Vol 23J (1999) 1197

[16]   D. Reiter et al., Plasma Phys. Contr. Fusion **33** (1991) 1579

[17]   G. Haas et al., J. Nucl. Mater. **196-198** (1992) 481.

[18]   U. Fantz et al., these proceedings

[19]   R. K. Janev, T. Kato and J. G. Wang, submitted for publication in Physics of Plasmas

#17824, f_{exp} = 2.8   #17823, f_{exp} = 6.4   #17822, f_{exp} = 9.3
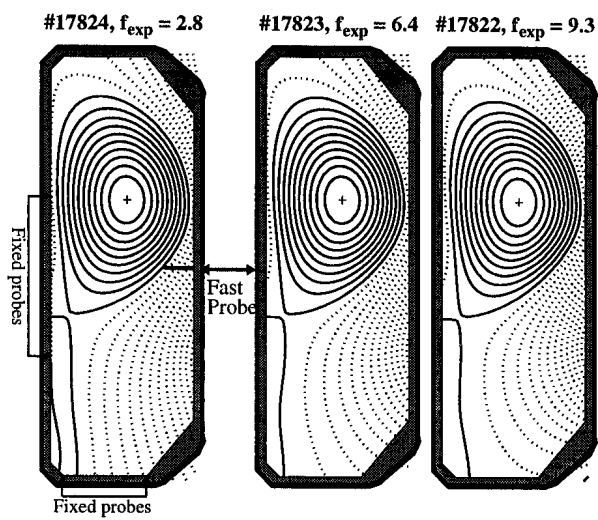
Fixed probes

Fast Probe

Fixed probes

Fig. 1. Illustrating the range of outer divertor flux expansion investigated in this study and showing the extremely short and long X-point to target poloidal distances for the inner and outer divertors respectively. The location of Langmuir probe diagnostics is also indicated. All equilibria plotted at t = 0.8 s.
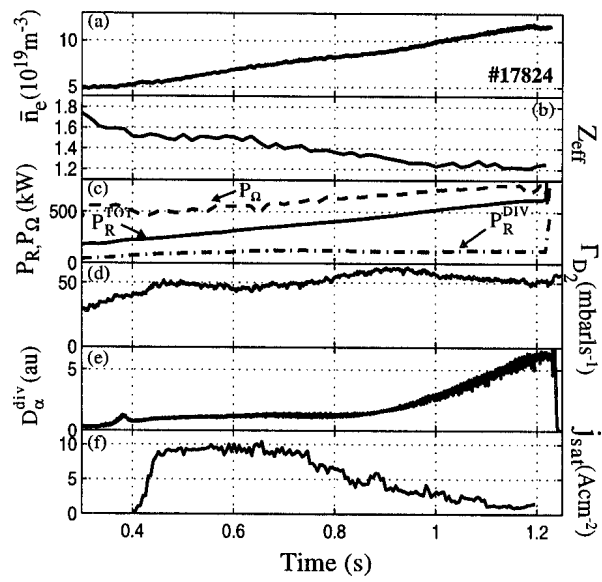
Fig. 2. Time variation of some relevant plasma signals for a typical density ramp detachment discharge.
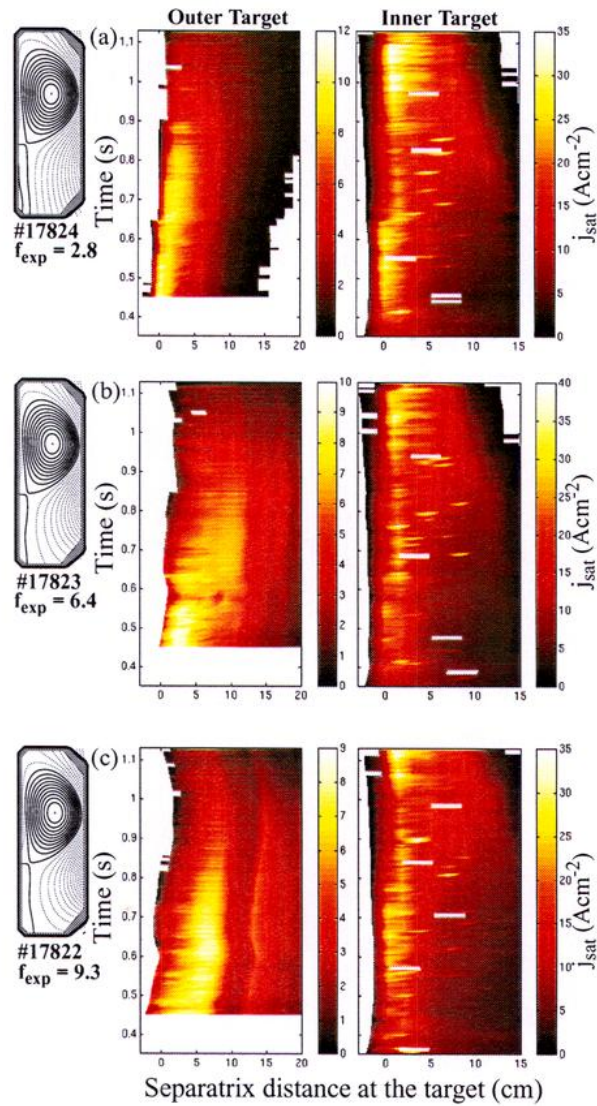
Fig. 3. Time dependent profiles of ion current density to the inner and outer targets for the three equilibria of Fig. 1. White areas in each plot correspond to the absence of data. The "deeper" and earlier detachment with increasing f_{exp} can be clearly seen, along with probe shadowing effects at high f_{exp}.
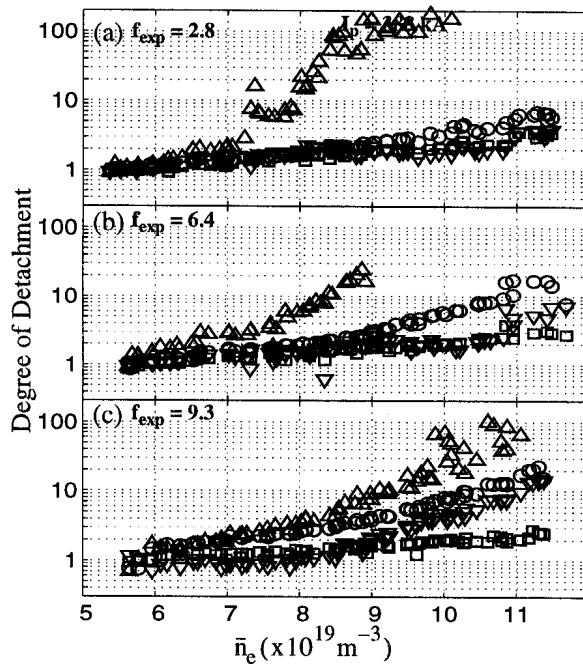
Fig. 4. Illustrating the effect of outer flux expansion and plasma current on the degree of separatrix and integral ion flux detachment for both inner and outer divertor targets. The symbols have the following meaning: $\bigcirc$: Outer divertor, integral current, $\square$: Inner divertor, integral current, $\triangle$: Outer divertor, separatrix current density, ∇: Inner divertor, separatrix current density
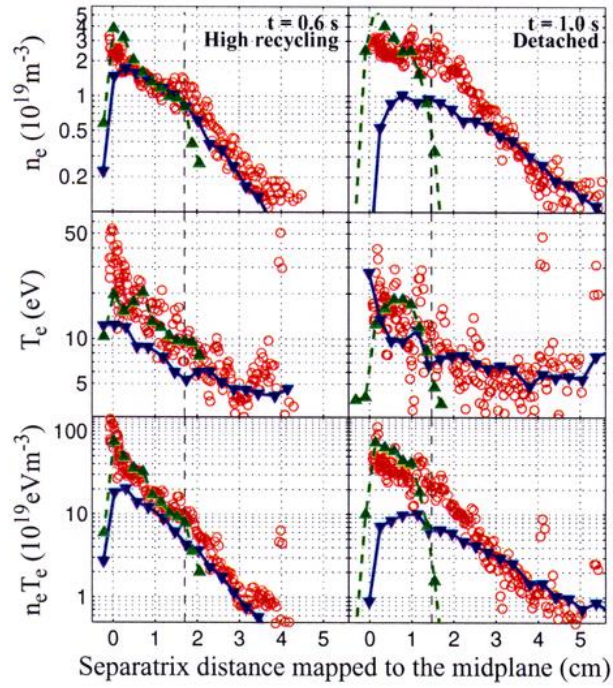
Fig. 5.   Profiles of n_e, T_e and p_e for both the divertor probe arrays and the reciprocating probe at low outer divertor f_{exp} (TCV shot #17824). The data are plotted in terms of distance from the separatrix mapped to the outer midplane. Red circles: reciprocating probe, blue full line: outer target probes, green dashed line: inner target probes. The triangle symbols mark the position of the indivdual divertor probes. The vertical dashed lines locate the outer wall tile radius at the midplane.
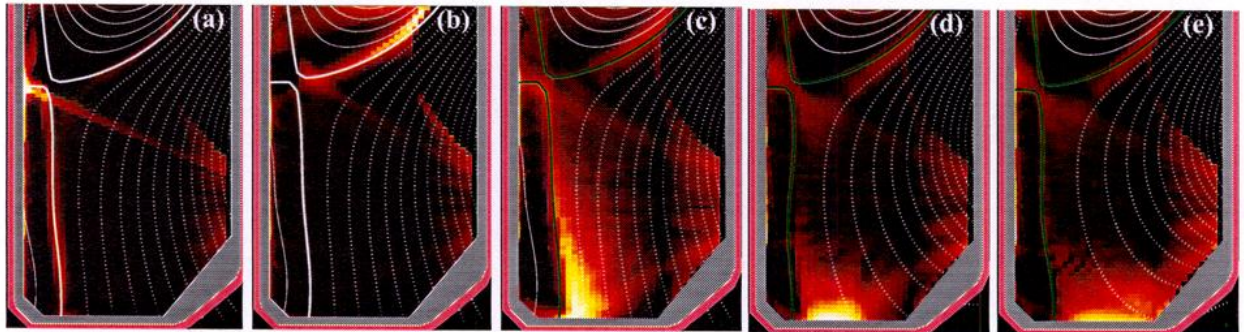
#17813, t = 0.50 s, CIII #17813, t = 1.18s, CIII #17824, t = 1.18 s, D_α #17823, t = 1.00 s, D_α #17822, t = 1.08 s, D_α

Fig. 6. Inverted visible CCD camera measurements of D_α (656 nm) and CIII (465 nm) emission in the divertor region. For the CIII emission the behaviour is independent of outer target flux expansion and examples from both the beginning and end of the density ramp (a,b) serve to illustrate how the difference in temperature distribution from high recycling to detached states influences the distribution of carbon radiation. In the case of the D_α (c,d,e), a single reconstruction from each flux expansion is shown at the time in the discharge for which outer target integral DOD's are similar (see text). The emission is uncalibrated, but is plotted within each group of images (CIII and D_α) on the same intensity scale for ease of comparison.
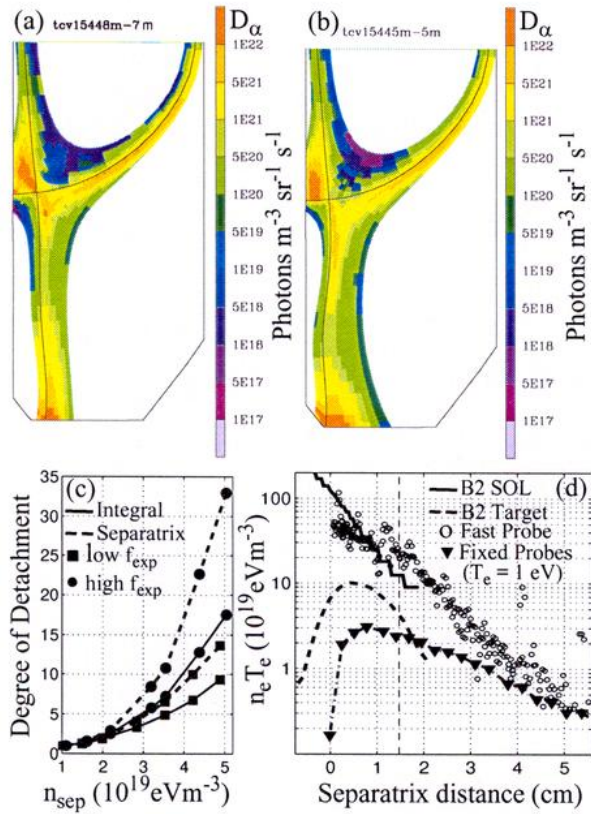
Fig. 7 Summary of selected B2-Eirene simulation results for the outer target and for low and high f_{exp} equilibria (TCV shots #15448, f_{exp} = 2.8 and #15445, f_{exp} = 6.4, I_p = 345 kA). The shape of the D_α distributions in (a,b), shown for similar absolute recombination levels, are in good agreement with the experimental data (see fig. 6 c,d). In (c), separatrix and integral DOD's for comparison with Fig. 4. (d) code outer target pressure profiles during detachment compared with fast probe and target profile data at 1.0 s from Fig. 5. The target probe data has been corrected for the electron temperature (T_e = 1 eV) predicted by the code at these densities.